AlN formation in Fe-Al alloys in N_2-O_2 atmospheres

J. H. Bott*, H. Yin, J. Zhu and S. Sridhar

The reheating of high aluminum content transformation-induced plasticity (TRIP) and light-weight steels in a nitrogen-rich atmosphere has been shown to cause development of subsurface aluminum nitride precipitates in addition to internal and external oxides. It is important to understand how these nitrides and oxides form and their consequences for the quality of steel products. This study looks at model iron-aluminum (up to 8 wt.% aluminum) alloys and uses confocal laser scanning microscopy, XRD, SEM-EDS, and TEM to study the effect of various conditions on the growth and development of these precipitates in a subsurface oxygen-depleted region. It was found that nitrides formed when bulk aluminum content was below 8 wt.% when oxygen was sufficiently depleted due to the internal oxidation. In the samples containing 1 wt.% aluminum, the depth of the internal oxide and nitride zones were in agreement with the model proposed by Meijering. Increasing aluminum content to 3 and 5 wt.% had the effects of modifying the surface-oxide scale composition and increasing its continuity, which gradually decreased the internal precipitation zones with increasing aluminum content. In samples containing 8 wt.% aluminum, a thick continuous oxide sale formed and completely prevented nitrogen and oxygen penetration into the bulk of the sample, thus preventing the formation of any internal precipitates.

1 Introduction

Transformation-induced plasticity (TRIP) steels are grades of steel used in automotive applications for their superior formability and high strength. They typically contain 0.1–0.2 wt.% carbon, 1.0–2.2 wt.% silicon, and 1.0–3.0 wt.% manganese [1]. The silicon is present to inhibit the formation of iron carbides and allow for carbon enrichment in the austenite [2], but its presence leads to problems during galvanization because of the difficulty of removing silicon-based oxides [3,4]. Up to about 1.5% aluminum has been considered as a replacement for silicon in order to improve galvanizability. Twinning-induced plasticity (TWIP) grade steels exhibit similar galvanization problems and can have aluminum contents up to about 6% [5,6]. Though aluminum additions improve galvanizability, iron-aluminum alloys are known to develop aluminum nitride precipitates when exposed to high temperatures in nitrogen-containing environments. This project intends to study the formation of aluminum nitrides in model iron-aluminum alloys.

Nitrogen and oxygen from the air and water vapor from spray nozzles are present during continuous casting. Furthermore, nitrogen, oxygen, and water vapor are present in the post-casting reheating environment as a result of the combusted furnace gas as the steel is prepared for hot-rolling. The gaseous species react with the high-aluminum content alloys to form an oxide scale and internal oxide and nitride inclusions.

These inclusions are thought to cause several problems during the processing of the steel. First, the internal aluminum nitride particles contribute to crack initiation in the sheet product because of particle-matrix interfacial separation. The aluminum nitride inclusions are also thought to weaken grain boundaries and thereby decrease the hot ductility of TRIP alloys. Additionally, aluminum nitride precipitates have been shown to pin austenite grain boundaries, which could affect grain growth during casting and subsequent heat treatments [7]. This study looks at the reheating regime prior to hot rolling, and nitrides formed during this reheat could detrimentally affect grain structure going into the hot rolling processes. The objective of the study is to document the conditions under which the nitrides form, but at this state it is not the intention to establish the detrimental roles they may have on materials properties.

J. H. Bott, J. Zhu
Department of Materials Science and Engineering, Carnegie Mellon University, Pittsburgh, PA 15212 (USA)
E-mail: jbott@andrew.cmu.edu

H. Yin
ArcelorMittal Global R&D, East Chicago, IN 46321, (USA)

S. Sridhar
University of Warwick, Warwick Manufacturing Group, International Digital Laboratory, Coventry, CV4 7AL, (UK)

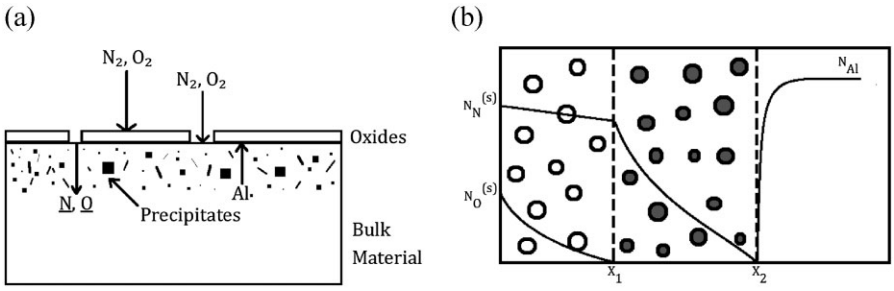

Figure 1. Schematics of diffusion processes. (a) Schematic of diffusion processes. (b) Precipitate penetration depth and solute concentrations (after Ref. [10])

This investigation seeks to elucidate the fundamental understanding of the kinetics and thermodynamics of this system, which will provide insight into techniques that may be able to control the development of these particles in high-aluminum content TRIP and TWIP steels.

If there are sufficient levels of aluminum and nitrogen in the system, they will combine to form aluminum nitride. The thermodynamically stable form of aluminum nitride is a hexagonal wurtzite structure. However, oxide films, if dense and continuous, are known to severely limit the penetration of adsorbed nitrogen into the bulk of the material, since the solubility of nitrogen is low in the oxide [8]. This, of course, assumes that the oxides can prevent molecular transport by being completely gas tight. The resistance of the oxide scale to molecular transport will depend on the microstructure. Oxides may develop on and below the surface of the material.

Figure 1 shows a sketch of the envisioned diffusion processes occurring within samples in this study. The oxygen potential in these initial studies will be sufficiently high for the conditions to become unfavorable for selective oxidation of aluminum. Therefore, iron and iron-aluminum oxides will likely form on the surface. The free energy of formation of alumina is far lower than that of aluminum nitride. Therefore, as shown in Fig. 1b the internal oxides will first form below the surface and the nitrides will be expected to appear only at locations where the oxygen activity is sufficiently low and the nitrogen activity sufficiently high (beyond the critical depth, X_1) and will extend to a depth X_2. Above X_1, the more thermodynamically stable aluminum oxide will form.

This study investigates the formation of surface scales and sub-surface precipitates of model Fe-Al alloys in N_2-O_2 environments during thermal conditions similar to those during reheating prior to hot-rolling. Water vapor and CO_2 are excluded in this initial study in order to simplify the analysis. The hypothesis of the present study is that, under the experimental conditions in this study, the nitrogen activity is sufficiently high at locations below the surface to allow for the precipitation of aluminum nitride. The formation of this nitride layer can be explained by a diffusion model that assumes gas access to the metal surface, i.e. that the top oxide scale is permeable. This permeability will cease at a critical aluminum content at which the outer scale is sufficiently compact and nitrides will be absent.

2 Experimental procedure

2.1 Materials

Four compositions were studied. The composition of each heat was analyzed at ArcelorMittal Indiana Harbor using induction coupled plasma mass spectrometry for aluminum and manganese content and LECO combustion analysis for carbon and nitrogen content and is listed in Table 1. The 3 wt.% and 5 wt.% aluminum samples were found to contain small amounts of carbon and manganese (<0.2 wt.%). Manganese is known to stabilize γ-iron [5] and is calculated in FactSage [9] to react with oxygen in a manner similar to iron by forming manganese aluminate and manganese oxide. Each heat was cast in 12.7 cm × 12.7 cm × 30.5 cm ingots and samples were cut from the interior of the ingot. To study the starting microstructure, an untreated 1 wt.% aluminum sample was etched in a 5% nitric acid – 95% methanol solution, which revealed very large ferrite grains (>2 mm), as shown in Fig. 2. All other samples had large grain size. While this large grain structure is not ideal for quantifying the possible effects of grain-boundary diffusion, it does represent an "as-cast" structure prior to hot-rolling.

Table 1. Sample compositions

Nominal aluminum content	Al (wt.%)	N (ppm)	C (wt.%)	Mn (wt.%)	S (wt.%)	Si (wt.%)
1 wt.%	1.062	3	<0.002	–*	<0.002	–*
3 wt.%	3.002	6	0.1516	0.173	0.001	0.011
5 wt.%	4.886	8	0.1493	0.171	0.001	0.016
8 wt.%	8.044	3	<0.002	–*	<0.002	–*

Compositions marked with an asterisk (*) were not measured.

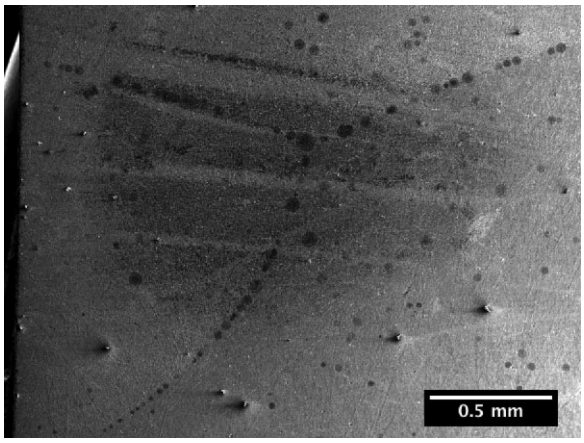

Figure 2. Etched untreated 1 wt.% Al sample

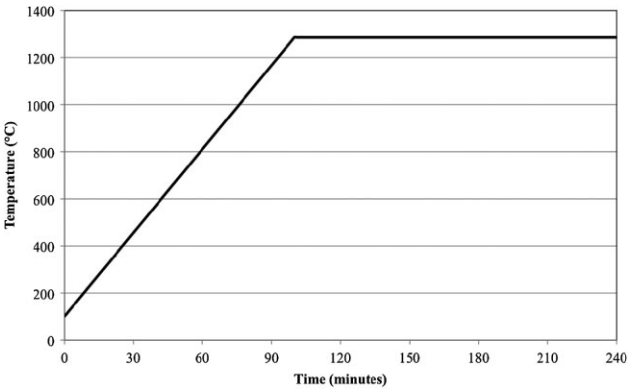

Figure 3. Experimental time-temperature profile

2.2 Experimental method

Experiments were performed in a nitrogen atmosphere to maximize the effects of aluminum content and time on aluminum nitride formation and minimize the role of the external scale. The nitrogen gas was 99.995% pure, with oxygen and water vapor impurities. The partial pressure of oxygen in the nitrogen gas used in these experiments was measured with a doped zirconia-based oxygen sensor to be 1.5×10^{-6} atm. Another set of experiments was performed using a mix of argon – 10% nitrogen to study the effect of nitrogen pressure.

The samples were polished to a 1 μm finish before heat treatment to remove any pre-existing oxides and to provide an adequate surface for viewing in the confocal laser scanning microscope (CLSM). Each sample was then loaded in an alumina crucible and placed in a sealed, radiation-heated furnace attached to the CLSM for heat treatment. This Au-image furnace allows samples to be heated and cooled with fine temperature control, including rapid heating and cooling, by adjusting the power provided to the halogen bulb heat source.

The heat treatment regime was designed to replicate a TRIP steel slab reheating process and is shown in Fig. 3. The temperature was ramped from room temperature to 1285 °C over the course of 100 min. The industrial slab reheating process then required the slab to be held at 1285 °C for an additional 80–300 min. In the present experiments, the samples were either rapidly cooled (around −10 K/s) in the N_2 atmosphere immediately after the initial heating or held at temperature for additional time and then cooled. Table 2 lists the experiments performed.

1 wt.% aluminum samples are expected to undergo a phase transformation α-iron to γ-iron during the heating. 3 wt.%, 5 wt.%, and 8 wt.% aluminum samples remain α-iron throughout the present temperature range.

2.3 Characterization methods

Characterization was performed on untreated samples using scanning electron microscopy (SEM) on etched samples. Samples that were difficult to etch were observed using electron backscatter scanning diffraction (EBSD). This technique can distinguish grains of different orientations, which allows for the characterization of microstructure.

Characterization was performed on the surface and cross-section of each sample after heat treatment. X-ray diffractometry (XRD) and SEM with energy dispersive X-ray spectroscopy (EDS) were used to determine the composition of the predominant oxide phases and to observe their morphology. SEM-EDS was used to determine the composition of the sub-surface scale layers and precipitates. Focused ion beam milling technology (FIB) was used to extract specimens for a more detailed transmission electron microscopy (TEM) phase analysis using electron diffraction and scanning transmission electron microscopy (STEM) coupled with EDS.

Table 2. Matrix of experiments

Experiment name	Alloy composition (%)	Gas	Heating time (min)	Isothermal time (min)	Isothermal temperature (°C)
Fe1Al-N2-100	1	N_2	100	0	1285
Fe1Al-N2-300	1	N_2	100	200	1285
Fe1Al-N2-400	1	N_2	100	300	1285
Fe1Al-10N2-300	1	10% N_2	100	200	1285
Fe3Al-N2-100	3	N_2	100	0	1285
Fe3Al-N2-300	3	N_2	100	200	1285
Fe5Al-N2-100	5	N_2	100	0	1285
Fe5Al-N2-100	5	N_2	100	200	1285
Fe8Al-N2-100	8	N_2	100	0	1285
Fe8Al-N2-300	8	N_2	100	200	1285

3 Results and discussion

3.1 Effect of time

For compositions that do not contain manganese, the primary oxides are expected to be, according to thermodynamics, iron oxides (wüstite, magnetite), alumina, and hercynite, an iron-aluminum spinel phase ($FeAl_2O_4$). Samples containing manganese were predicted to contain manganese and manganese-aluminum oxides. XRD and SEM-EDS scans of the surface show a discontinuous scale composed of magnetite, and wüstite, and hercynite (Table 3). Manganese-aluminum oxides are also found in the 3 wt.% and 5 wt.% aluminum samples.

Table 3. Scale compositions and thicknesses

Sample	Scale composition	Total scale thickness (μm)
Fe1Al-N2-100	Fe_3O_4, FeO, $FeAl_2O_4$	1
Fe1Al-N2-300	$FeAl_2O_4$, Fe_3O_4, FeO	>1
Fe1Al-N2-400	FeO, Fe_2O_3	1
Fe3Al-N2-100	Al_2O_3, $MnAl_2O_4$	1
Fe3Al-N2-300	Al_2O_3, $MnAl_2O_4$	2
Fe5Al-N2-100	$FeAl_2O_4$, $MnAl_2O_4$	<1
Fe5Al-N2-300	$FeAl_2O_4$, $MnAl_2O_4$	2
Fe8Al-N2-100	FeO, $FeAl_2O_4$, Fe_3O_4	5–6
Fe8Al-N2-300	$FeAl_2O_4$, Fe_3O_4, Al_2O_3	~3

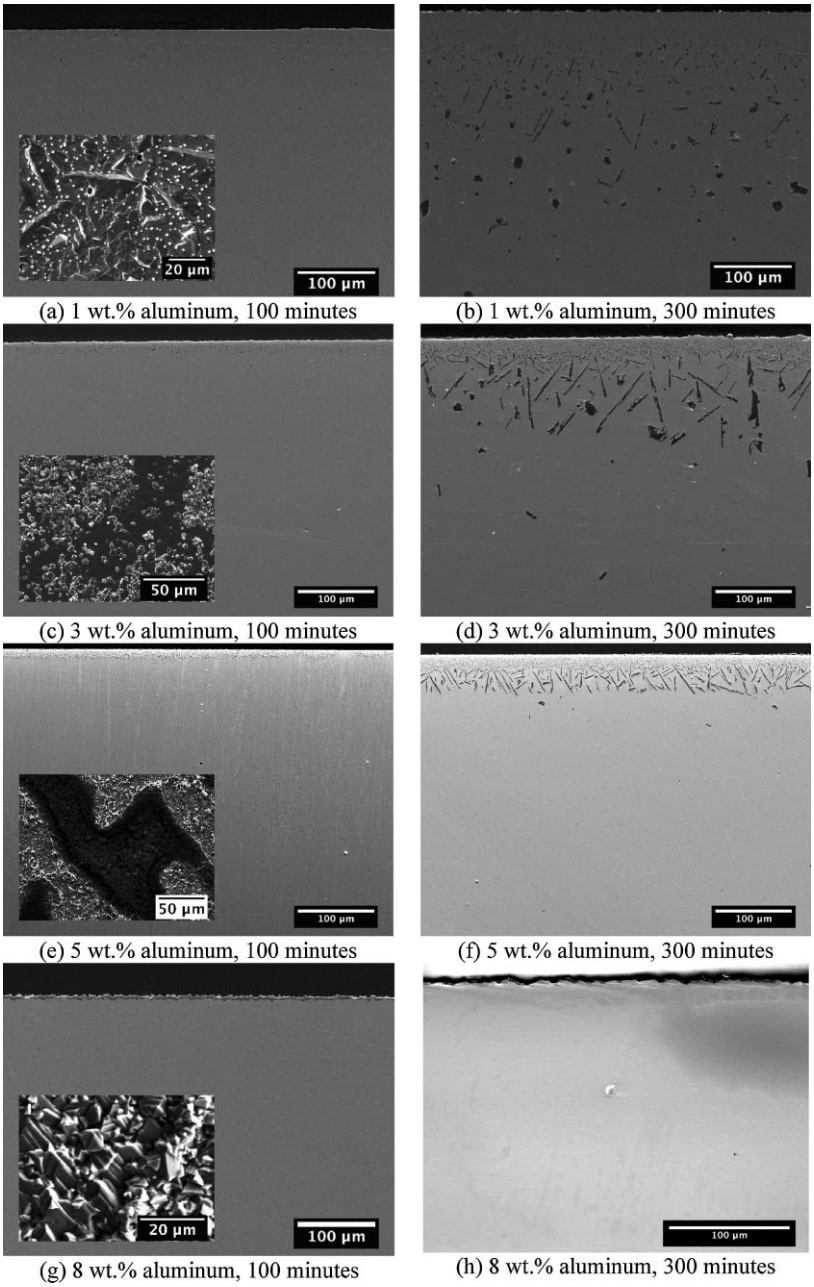

Figure 4. Cross-sectional SEM images of samples containing internal nitrides and oxides. Inlays are surface SEM images

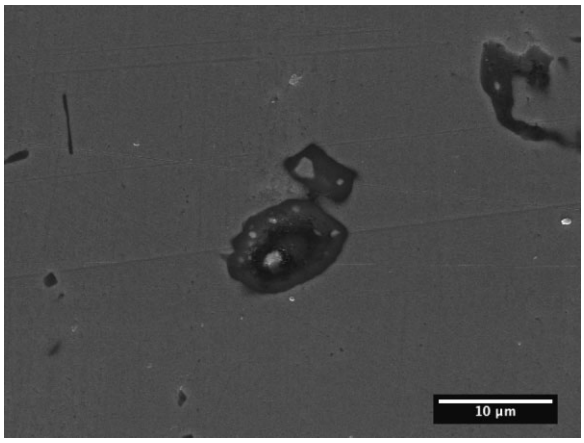

Figure 5. Detail of a mixed oxide/nitride particle from Fe1Al-N2-300

Large aluminum nitride particles were found in the 1 wt.%, 3 wt.%, and 5 wt.% aluminum samples. SEM micrographs of the cross-sections of samples from these three compositions are shown in Fig. 4. The precipitate penetration depth increases as time increases for each composition. For the 8 wt.% aluminum sample, internal precipitates were absent.

The 1 wt.% aluminum samples exhibited distinct layers of precipitates. SEM of the cross section (Fig. 4b) reveals a layer of internal oxides, followed by a layer of particles of mixed composition (Fig. 5), and subsequently, a layer of nitrides. TEM samples of the mixed particles in the intermediate layer were prepared using focused ion beam (FIB) techniques. TEM analysis reveals an inner aluminum nitride particle surrounded by a layer of alumina and then a layer of hercynite.

These mixed particles were likely produced by the moving diffusion fronts of oxygen and nitrogen. The moving oxygen front began to consume nitride particles previously formed by the leading nitride front. A schematic of this process is shown in Fig. 6.

Altering the duration of heat treatment had an effect on the depth of nitride and oxide layers, but was found to not alter the composition or morphology of the surface oxide in 1 wt.% aluminum samples. Precipitate penetration depths are listed in Table 4.

Hayashi and *Narita* [11] found a layer of subsurface needle-like hercynite particles and another layer of smaller needle-like aluminum nitride particles in 5 wt.% aluminum samples treated at 800 °C in air [11]. The hercynite particles in this study were

Table 4. Nitride layer penetration depths

Sample composition	Depth (µm)		
	100 min	300 min	400 min
1%-Al	250	500	870
3%-Al	20	180	–
5%-Al	15	50	–
8%-Al	0	0	–

arrayed with their long axis mostly perpendicular to the surface, whereas the aluminum nitride particles had a variety of orientations.

Focused ion beam milling technology was used to extract TEM samples of the internal precipitates, which were too small to characterize with SEM-EDS. In particular, particles with a seemingly mixed composition (as in Fig. 5) and the needle-like oxide particles were studied. These particles and their location with respect to the layers of oxides and nitrides in the sample are shown in Fig. 7. Additionally, Fig. 7 shows diffraction patterns from various locations in the mixed oxide particle.

The mixed-oxide particles consisted of an internal aluminum nitride particle surrounded by a thin layer of fine-grained alumina and a thicker layer of hercynite. This particle can be seen to the right in Fig. 7. The aluminum nitride is found at the upper right-hand corner of the sample and each of the next layers is below and to the left of this particle.

The needle-like oxide precipitates were revealed to have a partially plate-like structure upon cross-sectioning in the FIB. This section can be seen at the bottom of Fig. 7. STEM with EDS revealed these particles to be mostly alumina, with small growths of hercynite within the particles. A small, round hercynite precipitate was also found.

3.2 Effect of composition

Increasing the aluminum content of the alloys significantly alters the scale composition and morphology, as well as the precipitate penetration depths and morphology (see Table 3 above).

In the 3 and 5 wt.% aluminum samples, the aluminum nitride particles appeared to be long, thin needles, whereas the cross-sections of the nitrides in the 1 wt.% aluminum samples were square. Additionally, the surface-scale composition shifted from primarily iron oxides to alumina and manganese-aluminum

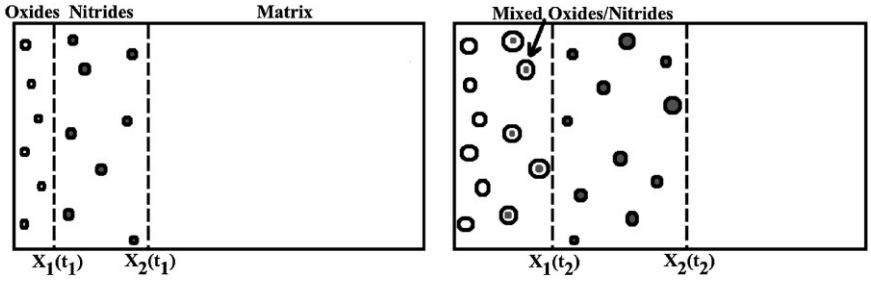

Figure 6. Schematic showing moving oxygen and nitrogen fronts (X_1 and X_2), where $t_1 < t_2$

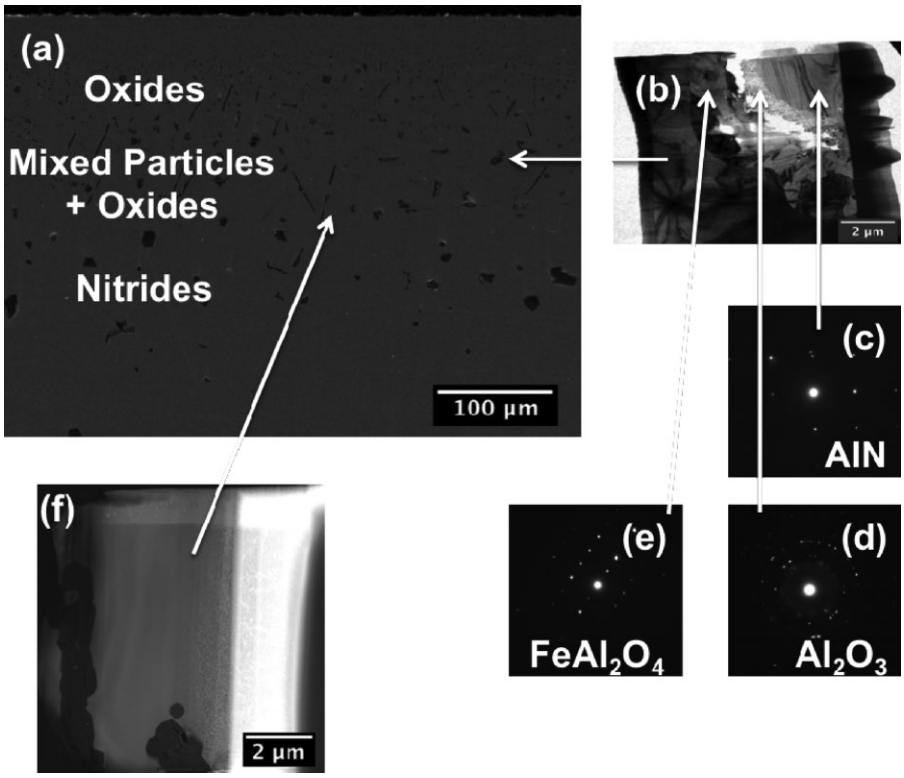

Figure 7. TEM micrographs and their location with respect to various layers of precipitates in 1 wt.% aluminum, 300 min sample. (a) SEM scattered electron micrograph of Fe1Al-N2-300, (b) TEM bright field of mixed oxide-nitride particle, (c–e) TEM diffraction patterns from mixed oxide-nitride particle, (f) STEM micrograph of needle-like oxide particles

oxides. The latter was due to the small Mn content in these samples. It should be noted that Mn was only found in the external scale and not in the internal precipitates.

Further increasing the aluminum content to 8 wt.% had the effect of eliminating internal precipitates. Each 8 wt.% sample had a thick, continuous surface scale comprised of an outer wüstite and/or magnetite layer, an inner hercynite layer, and possibly a thin inner-most layer of alumina. This scale corresponds well with scales seen in other oxidation studies on similar alloys [12–14].

Increasing the aluminum content in these experiments promotes the transition to external oxidation from internal oxidation, as analyzed by *Wagner* [15]. As no nitrides or internal oxides are seen in the 8 wt.% samples, it can be deduced that the presence of a thick, continuous external oxide scale limits the activity of oxygen at the scale-metal interface to a value which equals the dissociation pressure of the oxide nearest the interface, in this case alumina.

In particular, the alumina found in the scales on the higher aluminum content alloys is thought to have an important role in preventing oxygen and nitrogen penetration. Continuous alumina scales have long been known to be protective against further oxidation in iron-aluminum alloys. Several studies have been done to determine the critical aluminum content at which the alumina scale becomes protective [12,16–18]. This value varies depending on temperature and oxygen partial pressure. However, not all alumina scales are continuous and despite the initial growth of alumina scales, as time passes, iron oxide layers and nodules have been shown to develop and allow for internal oxidation [18].

3.3 Effect of varying P_{N2}

One sample was treated in a mixture of argon – 10% nitrogen (Fe1Al-10N2-300) instead of the pure nitrogen atmosphere. Scale and internal precipitate morphologies were unchanged, but both the nitride and oxide penetration depths were reduced. This reduction in penetration depth is further discussed below.

4 Analysis

4.1 Multiple internal precipitation model

A simple thermodynamic calculation shows that aluminum nitride is less stable than alumina and hercynite, and yet nitrides are frequently found in iron-aluminum alloys. For aluminum nitride to form, there must be a region in the sample where oxygen activity is very low. If the oxygen has been consumed in the process of forming oxides, the activity of oxygen in the alloy can be low enough to allow for the formation of nitrides.

An analytical model based on a multiple internal precipitation model developed by *Meijering* [19] confirms this supposition and accurately represents the 1 wt.% aluminum samples. Nitrogen and oxygen are taken as the two oxidative species in a binary iron-aluminum alloy. The model is modified so that the

Table 5. Thermodynamic data for precipitate phases

	Oxide phases		
	AlN [23]	Al_2O_3 [25]	$FeAl_2O_4$ [24]
Reaction	$AlN(s) = Al + N$	$^2/_3Al_2O_3 = 4/3Al + O_2$	$½FeAl_2O_4(s) = ½Fe(s) + Al(s) + O_2(g)$
$\triangle G^o(T)$	247,000–107.5T	1,111,733–213.3T	209,077–45.94T
$\triangle G_{1285\,^\circ C}$	79,515 J	784,960 J	137,510 J
	FeO [25]	Fe_3O_4 [25]	Fe_2O_3 [26]
Reaction	$2FeO(s) = 2Fe(s) + O_2(g)$	$2Fe_3O_4(s) = 6FeO(s) + O_2(g)$	$6Fe_2O_3(s) = 4Fe_3O_4(s) + O_2(g)$
$\triangle G^o(T)$	527,400–128.7T	622,200–228.7T	524,160–1769.36T
$\triangle G_{1285\,^\circ C}$	326,885 J	265,885 J	3,280,823 J

oxygen partial pressure at the surface is the equilibrium dissociation pressure of the oxide or spinel phases in the scale instead of the partial pressure in the gas. This is because the oxygen found in the nitrogen gas will react to form oxides at the iron surface. *Wallwork* [20] confirms the validity of this modification. The model shows that the less thermodynamically stable precipitate will be found deeper within the reaction zone of the sample than the more stable precipitate. The thermodynamic data in Table 5 confirm that aluminum nitride is the least stable among aluminum nitride, alumina, hercynite, wüstite, hematite, and magnetite.

The oxide penetration depth X_1 and the total precipitate penetration X_2 are found from Equations (1) and (2). The values for the diffusion coefficients of oxygen and nitrogen in austenite, D_O and D_N, respectively, were found in literature [21,22]. Using a nitrogen gas pressure of 1 atmosphere and 0.1 atmosphere, the solubility of nitrogen in austenite $N_N^{(s)}$ was also calculated from literature [8]. The terms ν_O and ν_N are stoichiometric terms relating the stoichiometry of oxygen or nitrogen in an oxide or nitride species to the aluminum content in that species.

The dissociation pressures of wüstite, hematite, magnetite, and hercynite in equilibrium with iron were calculated using the free energy values found in literature [24–26]. These values were used to calculate the solubility of oxygen in austenite, $N_O^{(s)}$ [24]. $N_{Al}^{(o)}$ is the initial concentration of aluminum in the alloy, i.e., 1 wt.%, which is approximately 2 atomic percent.

$$X_1^2 = 2\frac{D_O N_O^{(s)}}{\nu_O N_{Al}^{(o)}} t \quad (1)$$

$$X_2^2 = 2\left(\frac{D_O N_O^{(s)}}{\nu_O N_{Al}^{(o)}} + \frac{D_N N_N^{(s)}}{\nu_N N_{Al}^{(o)}}\right) t \quad (2)$$

It was assumed in these calculations that the initial 100-min heating to 1285 °C did not contribute to internal oxidation. The presence of internal oxide and nitride precipitates in the 100-min (zero-hold) sample shows that this is not true, but both the quantity and density of precipitates is very small and the nitride penetration depth in the 300-min sample is much larger at 500 μm compared to the sparse, uneven nitride front up to 250 μm in the 100-min sample. Therefore, the contribution of the 100-min heating is considered negligible for the purposes of this calculation. As nitrides do form, though, future work will be conducted to determine the effect of this 100-min heating period.

X_1 and X_2 as calculated from this model for each dissociation pressure are shown in Table 4. The values of X_1 and X_2 for wüstite and magnetite closely correspond to the measured values. Therefore, wüstite and/or magnetite likely control the oxygen partial pressure at the surface of the metal. Table 3 shows that either wüstite or magnetite or both oxides are present in each of the 1 wt.% aluminum samples.

The nitrogen pressure was reduced in one experiment to confirm that a reduction in N_N induces a decrease in the nitride precipitation depth as predicted by Equation (2).

The predicted values for X_2 correlate closely with measured values for 1 wt.% aluminum samples, as can be seen in Fig. 8 (using FeO as the partial-pressure controlling oxide) for the 300-min sample (200 min isothermal). The 400-min sample seems to develop precipitates more rapidly than the parabolic behavior predicted by the model. This could be a result of changes in the oxide scale composition and structure as time progresses, or of the development of some change in diffusivity as the precipitates develop during the isothermal period. Table 3 shows that the scale shifts to more iron-rich alloys for the 400-min sample.

X_1 values are less closely matched, possibly because of the effect of converting nitrides into oxides that results in the mixed particles found in the boundary region between the nitride and oxide regions. The mixed particle region spans approximately

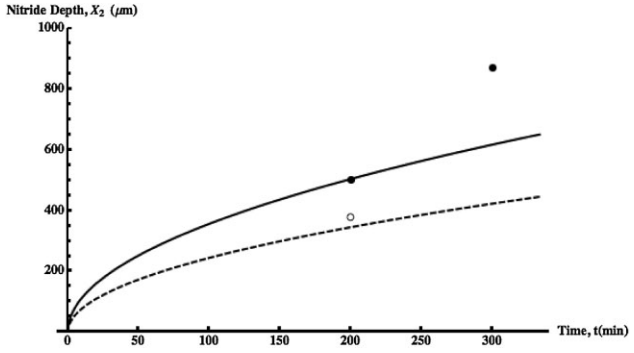

Figure 8. Measured *versus* predicted X_2 values for samples Fe1Al-N2-300, Fe1Al-N2-400, and Fe1Al-10N2-300 vs. isothermal annealing time (10%-N_2 sample is represented by the dashed line and open circle.)

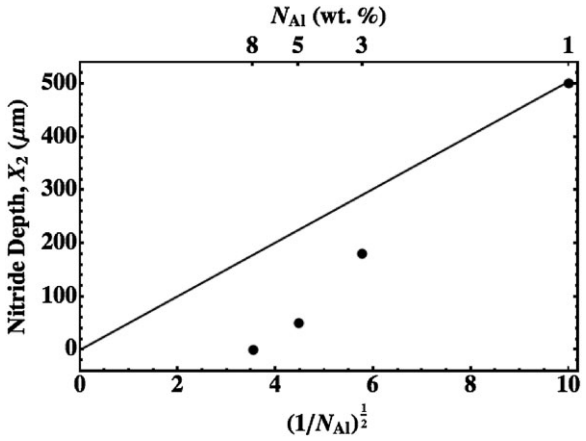

Figure 9. Predicted nitride penetration depth (X_2) *versus* measured values (dots) for various compositions

100 μm. This makes it hard to determine the exact size of the oxide region.

The predicted values for 3, 5, and 8 wt.% aluminum samples corresponded less closely to measured values than those for the 1 wt.% aluminum samples. Figure 9 shows the deviation from predicted values as aluminum content increases. The predicted X_2 values decrease for increasing aluminum content as given by Equation (2) for iron-aluminum alloys in equilibrium with a wüstite scale. The deviation from these values could be the result of several factors. First, upon formation of precipitates, it is possible that the interface between the particles and the matrix could provide a fast path for diffusion, which could affect the results of the model. Next, the model assumes the complete consumption of aluminum in the reaction zone to form precipitates, and therefore uses austenite diffusivity values to correspond to the pure iron matrix at experimental temperatures. In reality, there is no way to measure the aluminum content in the reaction zone over the course of the experiment, so it is possible that the use of the austenite diffusivity values is inaccurate. Additionally, as mentioned previously, the manganese found in the 3 and 5 wt.% aluminum samples can stabilize the austenite phase [5], so regardless of aluminum consumption in the reaction zone, the iron may be two-phase α/γ at reaction temperatures, which adds further inaccuracy to the calculation. Upon formation of precipitates, it is possible that the interface between the particles and the matrix could provide a fast path for diffusion, which could also affect the results of the model.

Perhaps the most important source for deviation is the change in scale composition for increasing aluminum content from mostly iron and iron-aluminum oxides to alumina and iron-aluminum oxides (see Table 3). Additionally, the increase in scale thickness from 1 μm to up to 6 μm and surface SEM micrographs (Fig. 4) shows that the oxide scales are more continuous for increasing aluminum content. Though the scales on the 3 and 5 wt.% samples are not as thick or continuous as those on the 8 wt.% samples, there is still a negative deviation from the predicted depths, indicating some effect of scale composition. It is clear that the decreased precipitation depth is greater than the predicted values. The role of increased aluminum could be in the thickness or structure of the external scale, which is critical for allowing ingress of gaseous nitrogen.

4.2 TEM analysis

TEM allowed for characterization of precipitates on a much smaller scale than SEM. Detailed study of particles at the boundary of the nitride and oxide regions revealed particles that contained both nitrides and oxides. The existence of such mixed phase particles shows that the conversion of aluminum nitride to alumina and hercynite is not a rapid one. Therefore these mixed particles introduce a complication to the use of the model, which assumes that the less stable species (aluminum nitride) is converted to the more stable species (alumina) rapidly. Additionally, it makes it more difficult to define X_1, where the oxide region ends.

The needle/plate-like alumina particles found in the oxide region further complicate matters, as their preferential growth perpendicular to the surface indicates some preference for oxygen diffusion along the interface between the particle and the matrix.

5 Conclusion

The present results support the hypothesis that nitride formation occurs because the nitrogen activity in the precipitation zone is large enough and the oxygen activity is low enough to form aluminum nitride in place of aluminum oxides. Increasing aluminum content had the effects of modifying the oxide scale composition and coverage, which slowed or prevented the formation of sub-surface oxides and nitrides. An analytical model supports these results and predicts the depth of oxide and nitride penetration for the 1 wt.% aluminum samples for isothermal annealing times of 200 min. When aluminum content is increased to 3 and 5 wt.% the measured depth at which nitrides appear is lower than what the model predicts, most likely due to the surface scale of alumina and/or manganese aluminate becoming more continuous. In samples containing 8 wt.% aluminum, a thick, continuous alumina-based scale formed and prevented nitrogen and oxygen penetration into the bulk of the sample, thus preventing the formation of precipitates.

Acknowledgements: The authors acknowledge ArcelorMittal Global R&D for their financial support and other in-kind support of this project. They would like to thank *E. Mantle* at ArcelorMittal Global R&D EC Center for making the lab ingots. The discussions with Dr. *O. Lanzi*, Dr. *S. Atreya*, and Dr. *S. Bhat*, all at ArcelorMittal Global R&D EC Center, were very valuable in the present study.

6 References

[1] T. L. Baum, R. J. Fruehan, S. Sridhar, *Metall. Mater. Trans. B* **2007**, *38*, 287.
[2] J. Gao, M. Ichikawa, *Proceedings of International Conference on Advanced High Strength Sheet Steels for Automotive Applications*, Winter Park, CO, June 6–9, **2004**, p. 107.

[3] T. Fukagawa, H. Okada, Y. Maehara, *ISIJ Int*. **1994**, *34*, 906.
[4] A. Chattopadhyay, T. Chanda, *Scr. Mater.* **2008**, *58*, 882.
[5] B. C. De Cooman, K. Chin, J. Kim, in: M. Chiaberge, (Ed.), *New Trends and Developments in Automotive System Engineering*, published online by InTech (http://www.intechopen.com/books/), **2011**.
[6] A. S. Hamada, *Ph. D. Thesis*, University of Oulu, Finland, **2007**.
[7] Ö. N. Dogan, G. M. Michal, H.-W. Kwon, *Metall. Mater. Trans. A* **1992**, *23A*, 2121.
[8] L. S. Darken, R. P. Smith, E. W. Filer, *Trans. Amer. Inst. Mining Met. Eng.* **1951**, *191*, 1174.
[9] C. W. Bale, A. D. Pelton, W. T. Thompson, *Facility for the Analysis of Chemical Thermodynamics*, Ecole Ploytechnique, Montreal, < http://www.factsage.com >, **2000**.
[10] D. J. Young, *High Temperature Oxidation and Corrosion of Metals*, Elsevier, Oxford **2008**.
[11] S. Hayashi, T. Narita, *Oxid. Met.* **2002**, *58*, 319.
[12] W. E. Boggs, *J. Electrochem. Soc.* **1971**, *118*, 906.
[13] S. Hayashi, T. Narita, *Oxid. Met.* **2001**, *56*, 251.
[14] S. Hayashi, T. Narita, *Nippon Kinzoku Gakkaishi* **1999**, *63*, 1311.
[15] C. Wagner, *Z. Elektrochem.* **1959**, *63*, 772.
[16] P. Tomaszewicz, G. R. Wallwork, *Oxid. Met.* **1983**, *19*, 165.
[17] H. A. Ahmed, W. W. Smeltzer, *J. Electrochem. Soc.* **1986**, *133*, 212.
[18] Z. G. Zhang, et al., *Corr. Sci.* **2006**, *48*, 271.
[19] J. L. Meijering, *Adv. Mat. Res. (N. Y.)* **1971**, *5*, 1.
[20] G. R. Wallwork, *Rep. Prog. Phys.* **1976**, *39*, 401.
[21] J. H. Swisher, E. T. Turkdogan, *Trans. Metall. Soc. AIME* **1967**, *239*, 426.
[22] P. Grieveson, E. T. Turkdogan, *Trans. Metall. Soc. AIME* **1964**, *230*, 407.
[23] Japan Society for the Promotion of Science. *Steelmaking Data Sourcebook: Revised Edition*, Gordon and Breach Science Publishers, New York **1988**.
[24] I. Barin, O. Knacke, O. Kubaschewski, *Thermochemical Properties of Inorganic Substances: Supplement*, Springer-Verlag, Berlin **1977**.
[25] D. R. Gaskell, *Introduction to the Thermodynamics of Materials*, Taylor and Francis, New York **2008**.
[26] M. W. Chase, Jr., NIST-JANAF Thermodynamic Tables, Fourth Ed., J. Phys. Chem. Ref. Data, Monogr., 9, **1998**, p. 1248.

(Received: June 17, 2013) W7257
(Accepted: July 1, 2013)

